Article

Photoinitiated Polymerization of Hydrogels by Graphene Quantum Dots

Yuna Kim [1,2,†], Jaekwang Song [1,2,†], Seong Chae Park [3,†], Minchul Ahn [1,2], Myung Jin Park [1,2], Sung Hyuk Song [4], Si-Youl Yoo [5], Seung Gweon Hong [5] and Byung Hee Hong [1,2,*]

[1] Department of Chemistry Seoul National University, Seoul 08826, Korea; ykim2189@gmail.com (Y.K.); saver04@snu.ac.kr (J.S.); mincheol@snu.ac.kr (M.A.); hanson2525@gmail.com (M.J.P.)
[2] Graphene Research Center, Advanced Institute of Convergence Technology, Suwon 16229, Korea
[3] Program in Nano Science and Technology, Graduate School of Convergence Science and Technology, Seoul National University, Seoul 08826, Korea; pscdaniel@snu.ac.kr
[4] Department of Mechanical Engineering, Seoul National University, Seoul 08826, Korea; shksong01023@gmail.com
[5] Interojo Inc., Pyeongtaek 17744, Korea; yoosy@interojo.com (S.-Y.Y.); steve.hong@interojo.com (S.G.H.)
* Correspondence: byunghee@snu.ac.kr
† These authors contributed equally to this paper.

Abstract: As a smart stimulus-responsive material, hydrogel has been investigated extensively in many research fields. However, its mechanical brittleness and low strength have mattered, and conventional photoinitiators used during the polymerization steps exhibit high toxicity, which limits the use of hydrogels in the field of biomedical applications. Here, we address the dual functions of graphene quantum dots (GQDs), one to trigger the synthesis of hydrogel as photoinitiators and the other to improve the mechanical strength of the as-synthesized hydrogel. GQDs embedded in the network effectively generated radicals when exposed to sunlight, leading to the initiation of polymerization, and also played a significant role in improving the mechanical strength of the crosslinked chains. Thus, we expect that the resulting hydrogel incorporated with GQDs would enable a wide range of applications that require biocompatibility as well as higher mechanical strength, including novel hydrogel contact lenses and bioscaffolds for tissue engineering.

Keywords: graphene quantum dots; hydrogel; organic-inorganic nanostructures; photoinitiator; photopolymerization

1. Introduction

Hydrogels, neither classified as completely liquid nor as solid state, are hydrophilic polymer networks which can absorb water to their porous networks. They have been of great interest to researchers in various applications such as polymer contact lenses and tissue engineering. The three-dimensional porous network structure can be modulated by controlling the ratio of monomers and crosslinking agents during polymerization. Moreover, the stimulus-responsive volume changes sensitive to temperature, pH, solvent, and electric field enables them to be applied in various biomedical applications [1–11]. In addition, the excellent optical and mechanical properties of the hydrogels can be applied to multifunctional contact lenses [12–14].

However, there have been some limitations of hydrogels for practical use. Firstly, they show poor mechanical properties with low tensile/compression strength and toughness. [5,15,16] Second, the conventional photoinitiators needed for hydrogel photopolymerization have an innate toxicity, limiting its usage in biological applications [17,18]. Thus, several methods have been proposed to synthesize hydrogels with enhanced mechanical properties and biocompatibility by hybridizing different nanomaterials [19–24]. Several carbon-based nanocomposites, such as carbon nanotubes, graphene oxides (GOs), or functionalized graphene sheets, have been implemented to improve the mechanical properties.

However, these carbon nanomaterials lack the ability to function as photoinitiators, and therefore, additional toxic substances need to be employed to generate the radicals to trigger the polymerization [16,22,25,26].

The photoinitiator should be a photosensitive molecule with an absorption wavelength range adequate for the initiation of polymerization reaction, and the absorbed photon should possess sufficient energy to generate free radicals. In this process, the functional groups on the initiator can expedite the polymerization reaction [27–29]. The graphene quantum dot (GQD), unlike the other graphene derivatives, is known to have distinctive optical properties showing size and edge-dependent fluorescence properties [24,30–38]. It shows wide absorption spectra ranging from UV to visible wavelengths. Furthermore, GQDs are expected to show better biocompatibility than other inorganic semiconductor nanoparticles such as TiO_2 and ZnO when they are used solely or as a composite [32,39–43].

Thus, we employed the dual functionality of GQDs as photoinitiators for the polymerization of polyacrylamide hydrogels and mechanical reinforcers of as-synthesized hydrogel networks (Scheme 1). They acted effectively even with sunlight as photoinitiators due to their broad absorption range, and achieved high Young's moduli by up to 50 times. The swelling ratio was similar or slightly increased compared to the hydrogel fabricated by the conventional photoinitiator. Finally, we demonstrated a potential application for contact lenses with high transmittance ($\geq$90%).
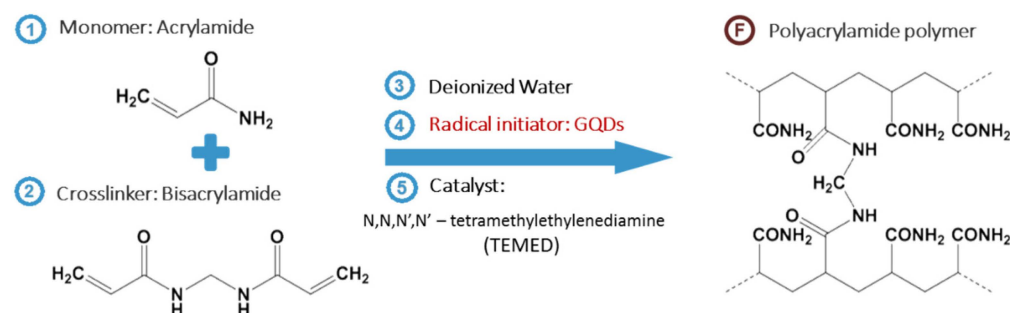
Scheme 1. Overall synthetic process of GQD-mediated hydrogel (GQDGel). The reactant (monomer and crosslinker) are dissolved in deionized water, followed by addition of initiator (GQD) and catalyst. After exposure to sunlight or UV, the final product, polyacrylamide hydrogel is synthesized.

2. Materials and Methods

2.1. Synthesis of GQDs

Graphene quantum dots (GQDs) were synthesized by following the previously reported method [32,40,41,44]. In brief, 0.9 g of carbon fiber was added into an acidic mixture of concentrated H_2SO_4 and HNO_3 in 3:1 (*v/v*) ratio. The mixed solution was sonicated for two hours and stirred for 24 h at 100 and 120 °C. The mixture was cooled and diluted with deionized (DI) water. The final product was then further dialyzed (molecular weight cut-off: 1 kDa) for 3 days, followed by lyophilization. Then, 0.01 g of as-fabricated GQD was mixed with 10 mL of DI water for its usage in hydrogel.

2.2. Characterization of GQDs

The GQD layers were characterized using various microscopic and spectroscopic techniques. Raman analysis was performed by inVia Raman Microscope (Renishaw, Gloucestershire, UK) An absorbance spectrum was obtained by UV−Vis-NIR spectrophotometer (S-3100, Scinco, Seoul, Korea). FT-IR spectra were acquired by FT-IR spectrophotometer (Nicolet 6700, Thermo Scientific, Waltham, MA, USA). The photoluminescence characterization was performed by the fluorescence spectrometer (FP-8300, Jasco Inc., Easton, MD, USA) with Xe lamp as the source of excitation.

2.3. Preparation of GQDGel and AGel

Acrylamide (AA) and *N*,*N*′-methylenebisacrylamide (MBAA) were dissolved in DI water with 40:1 and 400:1 of molar ratio. The solution was degassed in a vacuum chamber for 30 min. *N*,*N*,*N*′,*N*′-tetramethylethylenediamine (TEMED) was added into each solution, followed by addition of GQD solution (0.01 g/mL) or ammonium persulfate (APS) solution (0.01 g/mL). The solution was, finally, incubated under sunlight to be polymerized.

2.4. Dynamic Light Scattering (DLS) Analysis

The mixed solution was added to the cuvettes and exposed to the sunlight for polymerization. The measurement was carried out at room temperature with scattering angle of 275° by dynamic light scattering analyzer (Nano S, Malvern, Worcestershire, UK). The detailed calculation for DLS analysis is described in Supplementary Materials.

2.5. Mechanical Characterization of Hydrogels

Stress−strain curves for Young's modulus calculation were acquired by the universal testing system (INSTRON 5948, Instron, Norwood, MA, USA). A dog-bone shape of hydrogel specimen was fabricated for tensile test by ASTM D412. Hydrogel mixture solution was poured into the fabricated PDMS mold and left under the sunlight for polymerization. The tensile test for each specimen was performed with the 2 mm/min of extension. Surface adhesion force was measured by atomic force microscopy (XE-100, Park Systems, Suwon, Korea).

2.6. Electron Microscopy Analysis

Samples were lyophilized for scanning electron microscopy (SEM) observation. The dried AGel and GQDGel were cut into small pieces followed by Pt coating for SEM imaging. SEM observation was performed with 10 kV of operating voltage by field-emission SEM (JSM-6700F, JEOL Ltd., Tokyo, Japan). For tunneling electron microscopy (TEM) observation, a thin layer of solution was placed on TEM copper grid for direct polymerization and air-dried. TEM images were acquired by Cs-corrected TEM with Cold FEG (JEM-ARM200F, JEOL Ltd., Tokyo, Japan) with acceleration voltage of 80 kV.

3. Results and Discussion

First, several characterizations were performed to assure their photoresponsive properties and successful synthesis, such as Raman analysis, UV−Vis-NIR spectrophotometer, photoluminescence (PL) and Fourier-transform infrared (FT-IR) analysis (Figure 1). The Raman spectra of GQDs clearly showed two peaks, D (1350 cm^{-1}) and G (1605 cm^{-1}), indicating the successful synthesis of GQDs. In the absorbance spectrum, the peak around 250 nm was observed, which is related to π-π* transition of the conjugated C=C double bonds from graphitic characteristics of GQDs [45]. From the PL analysis, the emission peaks were observed at around 480 nm and 550 nm in all excitation range from 300 nm to 480 nm. In the FT-IR spectra, we could clearly observe several functional groups, such as carboxylic acid (1715 cm^{-1}), aromatic double bond (1610 cm^{-1}), ester (1236 cm^{-1}), and aromatic ether (1132 cm^{-1}); these functional groups are responsible for the high solubility of GQDs in water and for photoinitiation of polymerization purposes, as previously reported [32,40,41,44]. The wide range of photoresponsive properties of GQDs can be extensively used with a variety of light sources, even sunlight.
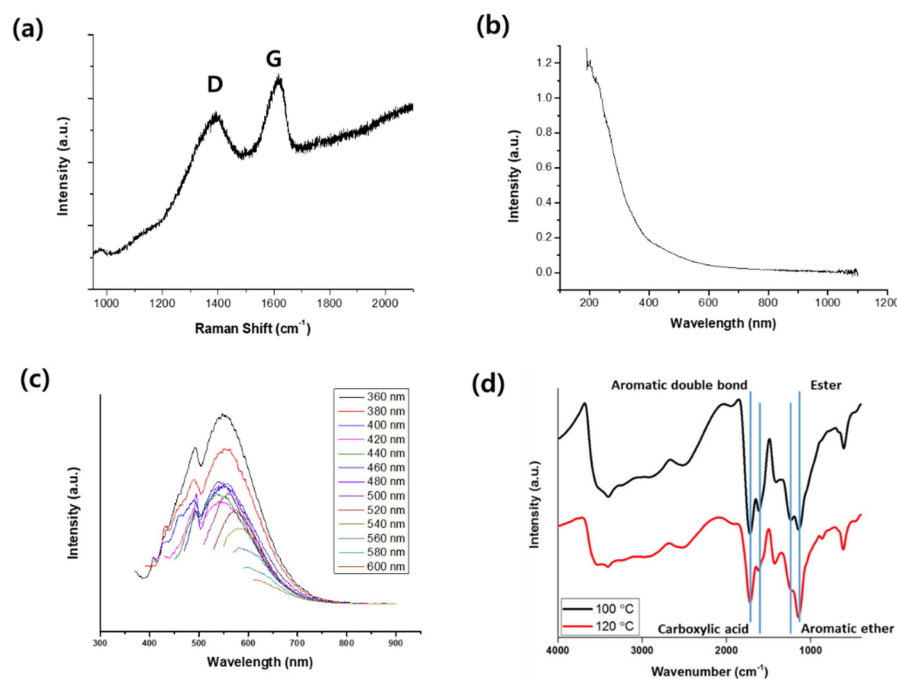
Figure 1. Characterization of graphene quantum dots. (**a**) Raman spectrum and (**b**) UV–Vis–NIR absorbance spectrum of GQD. (**c**) Emission spectra of GQDs with various excitation wavelengths. (**d**) FT–IR spectra of GQDs synthesized at 100 °C and 120 °C.

Light-responsive gelation with GQDs was confirmed by incubating the gelation solution either in a dark room or under sunlight. Incubation for 24 h in the dark room showed no indication of polymerization, but the sample after 20 min incubation under sunlight was transformed into the hydrogel (Figure 2a). In addition, we controlled the amount of GQD added in the gelation solution (Figure 2b,c). Ammonium persulfate (APS), a conventional photoinitiator for polymerization, was utilized to form hydrogels for comparison. All samples photoinitiated with GQDs and APS were transformed into hydrogels after exposure to sunlight as expected. On the other hand, no gelation was observed when GOs were employed as photoinitiators in the same conditions (Figure S1).

To confirm the sol−gel transition quantitively, dynamic light scattering (DLS) analysis for each sample was performed. DLS is one of the analysis tools for observing the dynamics or structural changes during gelation steps [46–50]. The detailed calculation method of DLS analysis for hydrogel is described in Supporting Information. The time-averaged intensity correlation function ($g^{(2)}(\tau)$–1), gelation factor κ, and dynamic structure factor S(q,τ) were plotted for AGel and GQDGels at the specific exposure time under sunlight, and sol−gel transition was clearly observed (Figure 3, Figure S2). Additionally, sol−gel transition of GQDGel_0.1 was confirmed by scanning electron microscopy (SEM) observation by exposure time (Figure S3). As the incubation time increased, the macromolecular structures from sol to gel state were observed. The walls of the polymers became smooth as no more active sites remained or as the reaction went to termination.
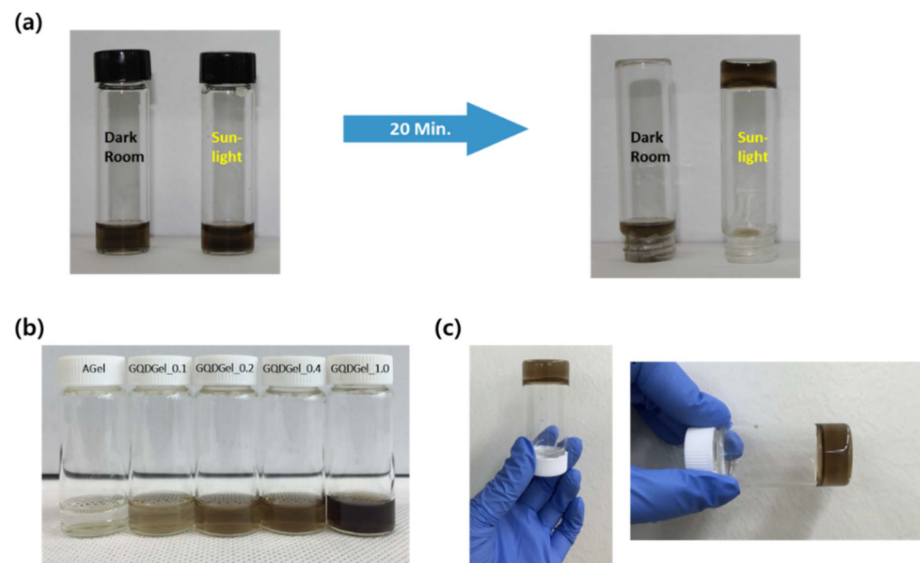
Figure 2. Photographs of the fabricated hydrogel samples. (**a**) Photographs of the GQD-incorporated gel samples before/after incubation in a dark room and under sunlight. (**b**) Photographs of the concentration-dependent gelation solutions. The numerical values on the labels (0.1, 0.2, 0.4, and 1) indicate the amount of GQD solution in mL included in the 3 mL of gelation solution. These values correspond to 0.0013, 0.0027, 0.0054, and 0.012 wt %, respectively. AGel, or APS-Gel, indicates the hydrogel formed by using ammonium persulfates as photoinitiator instead of GQDs. (**c**) Photographs of GQDGel_0.2 showing the successful gelation.
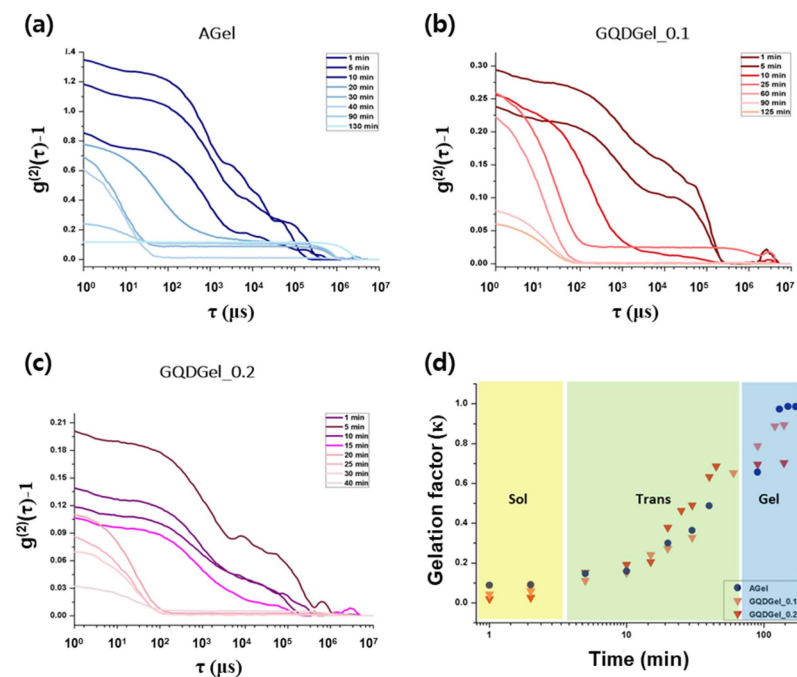

Figure 3. Dynamic light scattering analysis for hydrogel samples. time−intensity correlation function $(g^{(2)}(\tau)-1)$ of (**a**) AGel, (**b**) GQDGel_0.1, and (**c**) GQDGel_0.2 with increase of exposure time under sunlight. (**d**) Plot of gelation factor (κ) of each sample as a function of time.

To compare the microstructures of AGels with those of GQDGels, the cross-sectional view of AGel and GQDGel_0.2 samples were observed by SEM, which showed a highly porous structure with pore sizes ranging from a few to tens of micrometers (Figure 4). The pore size of the hydrogel was dependent on the ratio of monomer (AA) to crosslinking agent (MBAA); as the ratio of AA to MBAA increased, the pore size of the hydrogel

decreased. It is because a higher concentration of crosslinkers produce a large degree of polymer chain branches, resulting in the generation of additional networks. In addition, the amount of GQD hardly affected the pore structure, but the walls of the polymer network became thicker with an increased concentration of GQDs.
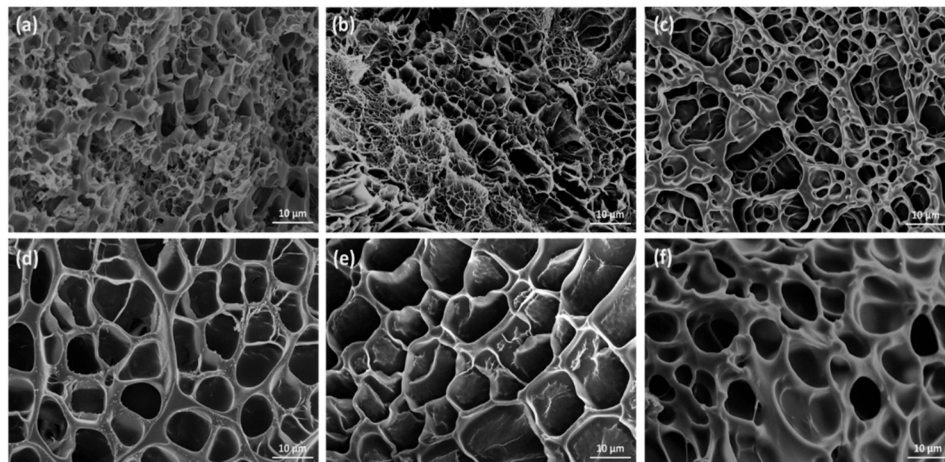

Figure 4. SEM images of the cross-sectional view of hydrogel samples. the porous structure of AA to MBAA ratio 40:1 of hydrogels (**a**) AGel, (**b**) GQDGel_0.2, and (**c**) GQDGel_0.4. and for AA to MBAA ratio 400:1 of hydrogels (**d**) AGel, (**e**) GQDGel_0.2, and (**f**) GQDGel_0.4 showing the enlarged pore size.

To confirm the embedment of GQDs in GQDGels, we performed Raman analysis of GQDGels, but only the characteristic Raman peaks of polyacrylamide were observed (Figure S4a). In order to directly isolate GQDs from GQDGels and run it through Raman analysis, we dissolved GQDGels with hydrogen peroxide solution, followed by dialysis and lyophilization (Figure S4b). Transmission electron microscopy (TEM) images also supported that GQDs were randomly dispersed and embedded within the polymer structure (Figure S5).

To verify the role of GQDs as mechanical reinforcers in the hydrogel structure, the fabricated hydrogel samples were prepared in a dog-bone shape for the tensile test (Figure 5a, Figure S6). Young's modulus of AGel slightly increased with the increased ratio of AA to MBAA component as previously reported, normally ranging from 10 to 30 kPa [51]. In contrast, the maximum Young's modulus of GQDGel_1.0 with 40:1 (AA:MBAA) ratio was measured as approximately 550 kPa, which was about 50 times larger than that of AGel with the same ratio. Next, we measured the surface adhesion force by atomic force microscopy (AFM), in which the pull-off force during the retraction of the AFM tips can inform about the free chemical chains on the surface of hydrogel. (Figure 5b, Figure S7) As shown from the mapping of the force-displacement measurement, the average of maximum surface adhesion force increased as the concentration of GQD increased. This is due to the addition of GQDs strengthening the hydrogel and also enhancing the adhesion force that is normally restrained on the hydrogel surface [16,19,25].
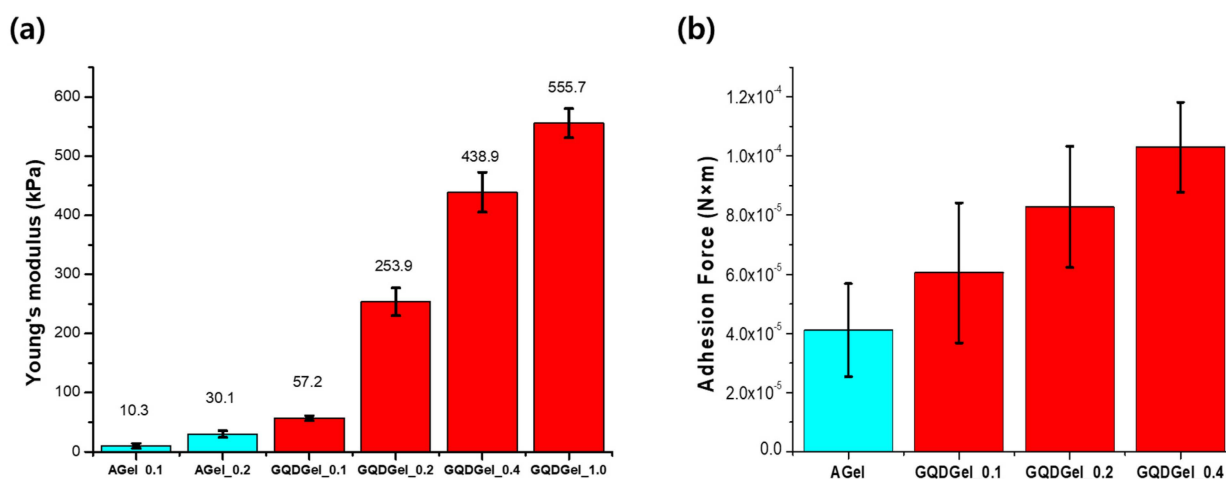
Figure 5. Mechanical characterization of the fabricated hydrogel. (**a**) Calculated Young's modulus for each sample. (**b**) Surface adhesion force of AGel and GQDGel samples measured by contact mode AFM measurement. The plotted values are the average of 10 μm × 10 μm measurement. All experiments were performed in triplicate.

Next, to define the fractional increase in the weight of the hydrogel due to water absorption, the swelling ratios of the fabricated hydrogel were measured (Figure 6). The swelling properties are usually affected by the network density, polymer-solvent interaction parameter, and by the pore size of the hydrogels [52–54]. The swelling ratio (Q) can be measured from the following Equation (1)

$$Q = \frac{W_{s,t} - W_d}{W_d} \times 100\%,$$ (1)

where $W_{s,t}$ is the weight of swollen hydrogel at time t and W_d is the weight of the dry hydrogel at t = 0. At the initial step, the swelling rate of GQDGel was about six times faster than that of AGel. We assume the hydrophilic functional groups on GQD contributed to increasing the swelling rate as well as the maximum swelling ratio of the hydrogel. The maximum swelling ratio of GQDGel was similar or slightly higher compared to AGel. However, when the excess amount of GQD was introduced during polymerization, the swelling ratio decreased. This is because the growing macromolecular chains are terminated at a faster rate as the concentration of initiator increases, resulting in the formation of low molecular-weight polymeric segments within the hydrogel network [52,54–56]. The excellent transparency as well as the controllable mechanical behavior and swelling property allowed our fabricated hydrogels to be potentially coapplied in the contact lenses or ocular drug delivery (Figure S8) [57–59].
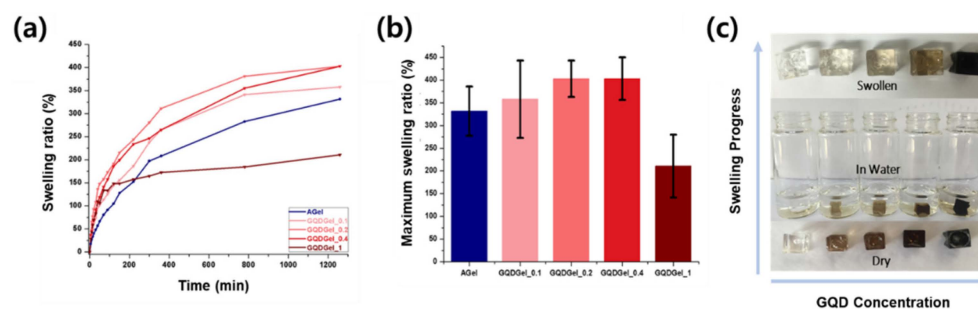

Figure 6. Swelling properties of hydrogel samples. (**a**) Calculated swelling ratio of each sample. (**b**) Average of maximum swelling ratio. The experiments were performed in triplicate. (**c**) Photograph of hydrogel swelling process from dry to swollen in DI water of AGel, GQDGel_0.1, GQDGel_0.2, GQDGel_0.4, and GQDGel_1, from left to right, respectively.

4. Conclusions

In summary, we synthesized chemically flexible and mechanically tough hydrogels using GQDs as photoinitiating reagents and confirmed that the unique photochemical properties of GQDs trigger the efficient crosslinking process of acrylamide monomers, enhancing its mechanical strength and swelling behaviors. Unlike GQDs, graphene oxides (GOs) were found to be inactive for the photoinduced polymerization of hydrogels. The dynamic light scattering (DLS) and electron microscopy (EM) analyses of the gelation steps indicate that the hydrogels were synthesized as GQD-embedded polymer matrices. As a result, Young's modulus and the surface adhesion the GQD-embedded hydrogels (GQDGel) were enhanced by 50 times and 2.5 times compared to the common AGel, respectively. The maximum swelling ratio of GQDGel was similar to that of AGel, but the excessive amount of GQDs that induced fast termination of polymerization reactions resulted in hardening and less swelling behaviors. We also demonstrated the potential application of the GQDGels to advanced contact lenses. In addition, the biocompatible GQD-based hydrogels with controllable mechanical properties and pore sizes as well as fluorescent properties would be useful for tissue engineering and drug delivery systems in the future.

Supplementary Materials: The following are available online at https://www.mdpi.com/article/10.3390/nano11092169/s1, Dynamic Light Scattering Analysis for Hydrogel; Figure S1: Photograph of hydrogel solution mixed with GQDs or graphene oxide before (top)/after (bottom) incubation in dark room or under sunlight. Incubation time in dark room was 24 h, while incubation under sunlight was 20 min. GO_0.2 and GO_0.4 are the gelation solutions with 0.2 and 0.4 mL of graphene oxide solution (0.01 g/mL), respectively, instead of graphene quantum dots., Figure S2: Derived dynamic structure factor of hydrogel samples. (a) GQDGel_0.1, (b) GQDGel_0.2, (c) AGel.; Figure S3: Scanning electron microscopy images of GQDGel_0.4 by exposure time. (a) Zero minutes (no irradiation), (b) 5 min, (c) 15 min, and (d) 30 min.; Figure S4: Raman spectra of (a) as-synthesized GQDGel and (b) GQDGel after post-treatment. Post-treatment is dissolving GQDGel by hydrogen peroxide solution, followed by dialysis and lyophilization to isolate GQDs from GQDGel.; Figure S5: (a–c) Transmission electron microscopy images of the GQDGel_0.1 sample with various magnifications.; Figure S6: Mechanical test for hydrogel samples. (a) Stress−strain curve for each sample. (b) Photograph of dog-bone shaped hydrogel specimen (left) and clamped specimen during the tensile testing process (right).; Figure S7: Surface adhesion energy measurement of hydrogel samples. (a) AGel, (b) GQDGel_0.1, (c) GQDGel_0.2, and (d) GQDGel_0.4 measured by AFM with the contact mode. The upper curves are the force deformation curve of cantilever: approach (black line) and retraction (red line). The bottom mapping is the adhesion force map of hydrogel samples of dimensions 10 μm × 10 μm. Number in the middle is the average of the adhesion forces measured from mapping.; Figure S8: Application of GQDGel in the simple contact lens. (a) Photographs of GQDGel_0.4 as a simple lens with the thickness of 0.1 mm. Left: without hydrogel lens, right: with hydrogel lens. (b) Transmittance of GQDGel_0.1 and GQDGel_0.4 in the visible range. The sample was polymerized in the contact lens mold with the thickness of 0.1 mm. (Inset: a photograph of polymerized lens in the mold for transmittance measurement).

Institutional Review Board Statement: Not applicable.

Informed Consent Statement: Not applicable.

Data Availability Statement: The data presented in this study are available on request from the corresponding author.

Conflicts of Interest: The authors declare no conflict of interest.

References

1. Wang, H.; Heilshorn, S.C. Adaptable Hydrogel Networks with Reversible Linkages for Tissue Engineering. *Adv. Mater.* **2015**, *27*, 3717–3736. [CrossRef]
2. Van Vlierberghe, S.; Dubruel, P.; Schacht, E. Biopolymer-Based Hydrogels as Scaffolds for Tissue Engineering Applications: A Review. *Biomacromolecules* **2011**, *12*, 1387–1408. [CrossRef] [PubMed]
3. Tomczykowa, M.; Plonska-Brzezinska, M.E. Conducting Polymers, Hydrogels and their Composites: Preparation, Properties and Bioapplications. *Polymers* **2019**, *11*, 350. [CrossRef]
4. Javadi, M.; Gu, Q.; Naficy, S.; Farajikhah, S.; Crook, J.M.; Wallace, G.G.; Beirne, S.; Moulton, S.E. Conductive Tough Hydrogel for Bioapplications. *Macromol. Biosci.* **2018**, *18*, 1700270. [CrossRef]
5. Li, J.; Mooney, D.J. Designing Hydrogels for Controlled Drug Delivery. *Nat. Rev. Mater.* **2016**, *1*, 16071. [CrossRef]
6. Hamidi, M.; Azadi, A.; Rafiei, P. Hydrogel Nanoparticles in Drug Delivery. *Adv. Drug Deliv. Rev.* **2008**, *60*, 1638–1649. [CrossRef] [PubMed]
7. Hoffman, A.S. Hydrogels for Biomedical Applications. *Adv. Drug Deliv. Rev.* **2012**, *64*, 18–23. [CrossRef]
8. Hunt, J.A.; Chen, R.; van Veen, T.; Bryan, N. Hydrogels for Tissue Engineering and Regenerative Medicine. *J. Mater. Chem. B* **2014**, *2*, 5319–5338. [CrossRef] [PubMed]
9. Nguyen, K.T.; West, J.L. Photopolymerizable Hydrogels for Tissue Engineering Applications. *Biomaterials* **2002**, *23*, 4307–4314. [CrossRef]
10. Rosiak, J.; Burczak, K.; Pekala, W. Polyacrylamide Hydrogels as Sustained-Release Drug Delivery Dressing Materials. *Radiat. Phys. Chem.* **1983**, *22*, 907–915. [CrossRef]
11. Billiet, T.; Vandenhaute, M.; Schelfhout, J.; Van Vlierberghe, S.; Dubruel, P. A Review of Trends and Limitations in Hydrogel-Rapid Prototyping for Tissue Engineering. *Biomaterials* **2012**, *33*, 6020–6041. [CrossRef]
12. Chatterjee, S.; Upadhyay, P.; Mishra, M.; Srividya, M.; Akshara, M.R.; Kamali, N.; Zaidi, Z.S.; Iqbal, S.F.; Misra, S.K. Advances in Chemistry and Composition of Soft Materials for Drug Releasing Contact Lenses. *RSC Adv.* **2020**, *10*, 36751–36777. [CrossRef]
13. Moreddu, R.; Vigolo, D.; Yetisen, A.K. Contact Lens Technology: From Fundamentals to Applications. *Adv. Healthc. Mater.* **2019**, *8*, 1900368. [CrossRef]
14. Driest, P.J.; Allijn, I.E.; Dijkstra, D.J.; Stamatialis, D.; Grijpma, D.W. Poly(Ethylene Glycol)-Based Poly(Urethane Isocyanurate) Hydrogels for Contact Lens Applications. *Polym. Int.* **2020**, *69*, 131–139. [CrossRef]
15. Gong, J.P.; Katsuyama, Y.; Kurokawa, T.; Osada, Y. Double-Network Hydrogels with Extremely High Mechanical Strength. *Adv. Mater.* **2003**, *15*, 1155–1158. [CrossRef]
16. Zhang, L.; Wang, Z.; Xu, C.; Li, Y.; Gao, J.; Wang, W.; Liu, Y. High Strength Graphene Oxide/Polyvinyl Alcohol Composite Hydrogels. *J. Mater. Chem.* **2011**, *21*, 10399–10406. [CrossRef]
17. Janney, M.A.; Omatete, O.O.; Walls, C.A.; Nunn, S.D.; Ogle, R.J.; Westmoreland, G. Development of Low-Toxicity Gelcasting Systems. *J. Am. Ceram. Soc.* **1998**, *81*, 581–591. [CrossRef]
18. Williams, C.G.; Malik, A.N.; Kim, T.K.; Manson, P.N.; Elisseeff, J.H. Variable Cytocompatibility of Six Cell Lines with Photoinitiators Used for Polymerizing Hydrogels and Cell Encapsulation. *Biomaterials* **2005**, *26*, 1211–1218. [CrossRef] [PubMed]
19. Arno, M.C.; Inam, M.; Weems, A.C.; Li, Z.; Binch, A.L.; Platt, C.I.; Richardson, S.M.; Hoyland, J.A.; Dove, A.P.; O'Reilly, R.K. Exploiting the Role of Nanoparticle Shape in Enhancing Hydrogel Adhesive and Mechanical Properties. *Nat. Commun.* **2020**, *11*, 1420. [CrossRef]
20. Huang, Z.-Y.; Barber, T.; Mills, G.; Morris, M.-B. Heterogeneous Photopolymerization of Methyl Methacrylate Initiated by Small ZnO Particles. *J. Phys. Chem.* **1994**, *98*, 12746–12752. [CrossRef]
21. Thoniyot, P.; Tan, M.J.; Karim, A.A.; Young, D.J.; Loh, X.J. Nanoparticle–Hydrogel Composites: Concept, Design, and Applications of these Promising, Multi-Functional Materials. *Adv. Sci.* **2015**, *2*, 1400010. [CrossRef]
22. Moniruzzaman, M.; Winey, K.I. Polymer Nanocomposites Containing Carbon Nanotubes. *Macromolecules* **2006**, *39*, 5194–5205. [CrossRef]
23. Zhang, D.; Yang, J.; Bao, S.; Wu, Q.; Wang, Q. Semiconductor Nanoparticle-Based Hydrogels Prepared via Self-Initiated Polymerization under Sunlight, even Visible Light. *Sci. Rep.* **2013**, *3*, 1399. [CrossRef]
24. Ruiz-Palomero, C.; Benítez-Martínez, S.; Soriano, M.L.; Valcárcel, M. Fluorescent nanocellulosic hydrogels based on graphene quantum dots for sensing laccase. *Anal. Chim. Acta* **2017**, *974*, 93–99. [CrossRef]
25. Chatterjee, S.; Lee, M.W.; Woo, S.H. Enhanced Mechanical Strength of Chitosan Hydrogel Beads by Impregnation with Carbon Nanotubes. *Carbon* **2009**, *47*, 2933–2936. [CrossRef]
26. Bai, H.; Sheng, K.; Zhang, P.; Li, C.; Shi, G. Graphene Oxide/Conducting Polymer Composite Hydrogels. *J. Mater. Chem.* **2011**, *21*, 18653–18658. [CrossRef]
27. Ge, J.; Lan, M.; Zhou, B.; Liu, W.; Guo, L.; Wang, H.; Jia, Q.; Niu, G.; Huang, X.; Zhou, H.; et al. A Graphene Quantum Dot Photodynamic Therapy Agent with High Singlet Oxygen Generation. *Nat. Commun.* **2014**, *5*, 4596. [CrossRef]
28. Zhou, Y.; Sun, H.; Wang, F.; Ren, J.; Qu, X. How Functional Groups Influence the ROS Generation and Cytotoxicity of Graphene Quantum Dots. *Chem. Commun.* **2017**, *53*, 10588–10591. [CrossRef] [PubMed]

29. Chatani, S.; Kloxin, C.J.; Bowman, C.N. The Power of Light in Polymer Science: Photochemical Processes to Manipulate Polymer Formation, Structure, and Properties. *Polym. Chem.* **2014**, *5*, 2187–2201. [CrossRef]

30. Tajik, S.; Dourandish, Z.; Zhang, K.; Beitollahi, H.; Van Le, Q.; Jang, H.W.; Shokouhimehr, M. Carbon and Graphene Quantum Dots: A Review on Syntheses, Characterization, Biological and Sensing Applications for Neurotransmitter Determination. *RSC Adv.* **2020**, *10*, 15406–15429. [CrossRef]

31. Moon, B.J.; Lee, K.S.; Shim, J.; Park, S.; Kim, S.H.; Bae, S.; Park, M.; Lee, C.-L.; Choi, W.K.; Yi, Y.; et al. Enhanced Photovoltaic Performance of Inverted Polymer Solar Cells Utilizing Versatile Chemically Functionalized ZnO@ Graphene Quantum Dot Monolayer. *Nano Energy* **2016**, *20*, 221–232. [CrossRef]

32. Peng, J.; Gao, W.; Gupta, B.K.; Liu, Z.; Romero-Aburto, R.; Ge, L.; Song, L.; Alemany, L.B.; Zhan, X.; Gao, G.; et al. Graphene Quantum Dots Derived from Carbon Fibers. *Nano Lett.* **2012**, *12*, 844–849. [CrossRef]

33. Konstantatos, G.; Badioli, M.; Gaudreau, L.; Osmond, J.; Bernechea, M.; De Arquer, F.P.G.; Gatti, F.; Koppens, F.H. Hybrid Graphene–Quantum Dot Phototransistors with Ultrahigh Gain. *Nat. Nanotechnol.* **2012**, *7*, 363–368. [CrossRef] [PubMed]

34. Li, M.; Chen, T.; Gooding, J.J.; Liu, J. Review of Carbon and Graphene Quantum Dots for Sensing. *ACS Sens.* **2019**, *4*, 1732–1748. [CrossRef] [PubMed]

35. Zhang, Z.; Chang, K.; Peeters, F. Tuning of Energy Levels and Optical Properties of Graphene Quantum Dots. *Phys. Rev. B* **2008**, *77*, 235411. [CrossRef]

36. Das, P.; Ganguly, S.; Banerjee, S.; Das, N.C. Graphene based emergent nanolights: A short review on the synthesis, properties and application. *Res. Chem. Intermed.* **2019**, *45*, 3823–3853. [CrossRef]

37. Ganguly, S.; Das, P.; Itzhaki, E.; Hadad, E.; Gedanken, A.; Margel, S. Microwave-Synthesized Polysaccharide-Derived Carbon Dots as Therapeutic Cargoes and Toughening Agents for Elastomeric Gels. *ACS Appl. Mater. Interfaces* **2020**, *12*, 51940–51951. [CrossRef] [PubMed]

38. Khabibullin, A.; Alizadehgiashi, M.; Khuu, N.; Prince, E.; Tebbe, M.; Kumacheva, E. Injectable Shear-Thinning Fluorescent Hydrogel Formed by Cellulose Nanocrystals and Graphene Quantum Dots. *Langmuir* **2017**, *33*, 12344–12350. [CrossRef]

39. Zhang, H.; Ba, S.; Yang, Z.; Wang, T.; Lee, J.Y.; Li, T.; Shao, F. Graphene Quantum Dot-Based Nanocomposites for Diagnosing Cancer Biomarker APE1 in Living Cells. *ACS Appl. Mater. Interfaces* **2020**, *12*, 13634–13643. [CrossRef]

40. Kang, I.; Yoo, J.M.; Kim, D.; Kim, J.; Cho, M.K.; Lee, S.-E.; Kim, D.J.; Lee, B.-C.; Lee, J.Y.; Kim, J.-J.; et al. Graphene Quantum Dots Alleviate Impaired Functions in Niemann-Pick Disease Type C In Vivo. *Nano Lett.* **2021**, *21*, 2339–2346. [CrossRef]

41. Lee, B.-C.; Lee, J.Y.; Kim, J.; Yoo, J.M.; Kang, I.; Kim, J.-J.; Shin, N.; Kim, D.J.; Choi, S.W.; Kim, D.; et al. Graphene Quantum Dots as Anti-Inflammatory Therapy for Colitis. *Sci. Adv.* **2020**, *6*, eaaz2630. [CrossRef]

42. Kim, D.; Yoo, J.M.; Hwang, H.; Lee, J.; Lee, S.H.; Yun, S.P.; Park, M.J.; Lee, M.; Choi, S.; Kwon, S.H.; et al. Graphene Quantum Dots Prevent α-Synucleinopathy in Parkinson's Disease. *Nat. Nanotechnol.* **2018**, *13*, 812–818. [CrossRef]

43. Shen, J.; Zhu, Y.; Yang, X.; Li, C. Graphene Quantum Dots: Emergent Nanolights for Bioimaging, Sensors, Catalysis and Photovoltaic Devices. *Chem. Commun.* **2012**, *48*, 3686–3699. [CrossRef] [PubMed]

44. Lee, B.-C.; Lee, J.Y.; Kim, J.; Shin, N.; Yoo, J.M.; Kang, I.; Kim, J.-J.; Lee, S.-E.; Kim, D.; Choi, S.W.; et al. Oral Administration of Microbiome-Friendly Graphene Quantum Dots as Therapy for Colitis. *2D Mater.* **2021**, *8*, 025036. [CrossRef]

45. Zhu, C.; Yang, S.; Wang, G.; Mo, R.; He, P.; Sun, J.; Di, Z.; Kang, Z.; Yuan, N.; Ding, J.; et al. A New Mild, Clean and Highly Efficient Method for the Preparation of Graphene Quantum Dots without By-Products. *J. Mater. Chem. B* **2015**, *3*, 6871–6876. [CrossRef] [PubMed]

46. Sabareesh, K.P.V.; Jena, S.S.; Tata, B.V.R. Dynamic Light Scattering Studies on Photo Polymerized and Chemically Cross-linked Polyacrylamide Hydrogels. In *AIP Conference Proceedings*; American Institute of Physics: College Park, MD, USA, 2006; Volume 832, pp. 307–310. [CrossRef]

47. Matsunaga, T.; Shibayama, M. Gel point determination of gelatin hydrogels by dynamic light scattering and rheological measurements. *Phys. Rev. E* **2007**, *76*, 030401. [CrossRef] [PubMed]

48. Asai, H.; Nishi, K.; Hiroi, T.; Fujii, K.; Sakai, T.; Shibayama, M. Gelation Process of Tetra-PEG Ion-Gel Investigated by Time-Resolved Dynamic Light Scattering. *Polymer* **2013**, *54*, 1160–1166. [CrossRef]

49. Rochas, C.; Geissler, E. Measurement of Dynamic Light Scattering Intensity in Gels. *Macromolecules* **2014**, *47*, 8012–8017. [CrossRef]

50. Kumar, N.; Kumar, V.; Sharma, J. Relaxations in Gelatin Hydrogels Probed by Dynamic Light Scattering. *Adv. Mater.* **2016**, *7*, 136–143. [CrossRef]

51. Kong, H.J.; Wong, E.; Mooney, D.J. Independent Control of Rigidity and Toughness of Polymeric Hydrogels. *Macromolecules* **2003**, *36*, 4582–4588. [CrossRef]

52. Bajpai, S.K.; Singh, S. Analysis of Swelling Behavior of Poly(Methacrylamide-co-Methacrylic Acid) Hydrogels and Effect of Synthesis Conditions on Water Uptake. *React. Funct. Polym.* **2006**, *66*, 431–440. [CrossRef]

53. Gerlach, G.; Guenther, M.; Sorber, J.; Suchaneck, G.; Arndt, K.-F.; Richter, A. Chemical and pH Sensors Based on the Swelling Behavior of Hydrogels. *Sens. Actuators B Chem.* **2005**, *111–112*, 555–561. [CrossRef]

54. Chen, J.; Zhao, Y. Relationship between Water Absorbency and Reaction Conditions in Aqueous Solution Polymerization of Polyacrylate Superabsorbents. *J. Appl. Polym. Sci.* **2000**, *75*, 808–814. [CrossRef]

55. Sadeghi, M.; Heidari, B. Crosslinked Graft Copolymer of Methacrylic Acid and Gelatin as a Novel Hydrogel with pH-Responsiveness Properties. *Materials* **2011**, *4*, 543–552. [CrossRef]

56. Hsu, S.-C.; Don, T.-M.; Chiu, W.-Y. Free Radical Degradation of Chitosan with Potassium Persulfate. *Polym. Degrad. Stab.* **2002**, *75*, 73–83. [CrossRef]
57. Zhang, Y.; Chen, Q.; Dai, Z.; Dai, Y.; Xia, F.; Zhang, X. Nanocomposite Adhesive Hydrogels: From Design to Application. *J. Mater. Chem. B* **2021**, *9*, 585–593. [CrossRef]
58. Li, F.; Zhang, G.; Wang, Z.; Jiang, H.; Yan, S.; Zhang, L.; Li, H. Strong Wet Adhesion of Tough Transparent Nanocomposite Hydrogels for Fast Tunable Focus Lenses. *ACS Appl. Mater. Interfaces* **2019**, *11*, 15071–15078. [CrossRef] [PubMed]
59. Dai, S.; Wang, S.; Dong, X.; Xu, X.; Cao, X.; Chen, Y.; Zhou, X.; Ding, J.; Yuan, N. A Transparent, Tough Self-Healing Hydrogel Based on a Dual Physically and Chemically Triple Crosslinked Network. *J. Mater. Chem. C* **2019**, *7*, 14581–14587. [CrossRef]